IEEE Access
Multidisciplinary | Rapid Review | Open Access Journal

Received 18 September 2023, accepted 10 October 2023, date of publication 16 October 2023, date of current version 25 October 2023.

Digital Object Identifier 10.1109/ACCESS.2023.3324670

RESEARCH ARTICLE

Finding Essential Parts of the Brain in rs-fMRI Can Improve ADHD Diagnosis Using Deep Learning

BYUNGGUN KIM[1], JAESEON PARK[1], TAEHUN KIM[1], AND YOUNGHUN KWON[1,2]
[1]Department of Applied Artificial Intelligence, Hanyang University, ERICA Campus, Ansan, Kyunggi-Do 425-791, Republic of Korea
[2]Department of Applied Physics, Hanyang University, ERICA Campus, Ansan, Kyunggi-Do 425-791, Republic of Korea

Corresponding author: Younghun Kwon (yyhkwon@hanyang.ac.kr)

This work was supported by the Basic Science Research Program through the National Research Foundation of Korea (NRF) funded by the Ministry of Education, Science and Technology, under Grant NRF2022R1F1A1064459.

ABSTRACT Although attention-deficit/hyperactivity disorder (ADHD) is a common psychiatric disorder, it is difficult to develop an accurate diagnostic method. Recently, studies to classify ADHD using resting-state functional magnetic resonance (rs-fMRI) imaging data have been conducted with the development of computing resources and machine learning techniques. Most of them use the entire brain's regions when training the models. As opposed to the common approach, we conducted a study to classify ADHD by selecting essential areas for using a deep learning model. The experiment used rs-fMRI data from the ADHD-200 global competition. To obtain an integrated result from the multiple sites, each region of the brain is evaluated using 'leave- one-site-out' cross-validation. As a result, when we only used 15 important regions of interest (ROIs) for training, 70.6% accuracy was obtained, significantly exceeding the existing results of 68.6% from all ROIs. Additionally, to explore the new structure based on SCCNN-RNN, we performed the same experiment with three modified models: (1) separate channel CNN - RNN with attention (ASCRNN), (2) separate channel dilate CNN - RNN with attention (ASDRNN), (3) separate channel CNN - slicing RNN with attention (ASSRNN). The ASSRNN model provides a high accuracy of 70.46% when trained with only 13 important ROIs. These results show that using deep learning to identify the crucial parts of the brain in diagnosing ADHD yields better results than using every area.

INDEX TERMS ADHD, deep learning, rs-fMRI, AAL116, ROI.

LIST OF ABBREVIATIONS

Abbreviations in this article are listed as follows.

Acronym	*Explanation*
AAL	Automated Anatomical Labelling atlas.
ASCRNN	Separate Channel CNN - RNN with Attention.
ASDRNN	Separate Channel Dilate CNN - RNN with Attention.
ASSRNN	Separate Channel CNN - slicing RNN with Attention.
ADHD	Attention-Deficit/Hyperactivity Disorder.
BHBU	Bradley/Brown University.
BiLSTM	Bidirectional Long Short-Term Memory.
BOLD	Blood-oxygen-level-dependent.
CNN	Convolutional Neural Network.
DNN	Deep Neural Network.
FC	Functional Connectivity.
HC	Healthy Control.
KKI	Kennedy Krieger Institute.
LOSO	Leave-One-Site-Out.
LSTM	Long Short-Term Memory.
MRI	Magnetic Resonance Imaging.
NI	NeuroIMAGE.
NIAK	Neuroimage analysis kit.
NYU	New York University.
OHSU	Oregon Health Sciences University.
ReLU	Rectified Linear Unit.
RNN	Recurrent Neural Network.

The associate editor coordinating the review of this manuscript and approving it for publication was Sotirios Goudos.

ROI	Region of Interest.
rs-fMRI	resting-state functional Magnetic Resonance Imaging.
SCCNN	Separate Channel Convolutional Neural Network.
SCDCNN	Separate Channel Dilate Convolutional Neural Network.
SER	Speech Emotion Recognition.
WUSTL	Washington University at Saint Louis.

I. INTRODUCTION

Attention-deficit/hyperactivity disorder (ADHD) is a psychiatric disorder that frequently appears in children [1], [2], [3]. However, until recently, there have been no specific tests for diagnosing ADHD [4]. To overcome this limitation, many studies have been conducted to identify a biomarker between healthy controls (HCs) and ADHD from medical data. For example, functional connectivity (FC) extracted from resting-state functional magnetic resonance imaging (rs-fMRI) data is frequently used with machine learning methods [5], [6], [7], [8], [9], [10], [11].

Owing to the recent exponential growth of deep neural network (DNN) model techniques, DNN-based models have been used to obtain the features of not only ADHD [12], [13], [14], [15], [16] but also other diseases [17], [18]. The deep learning models to diagnose ADHD using rs-fMRI can be divided into two categories according to the data characteristics. The first one is that after dividing a brain into specific regions and extracting features from rs-fMRI data of those regions, the deep learning model is trained by those features [12], [13], [14].

In these models, voxel-based feature or ROI-based feature is used. The former is the feature obtained from a brain divided by the same size. The latter is the feature obtained from various methods, such as functional connectome analysis. Those features can effectively reduce the data size of rs-fMRI and help effectively train deep learning models.

The second one is using all rs-fMRI data to train deep learning models [15], [16]. Even though this method uses massive data, unlike the first case, it can be more effective in training deep learning models than the first one.

However, we want to focus on the findings that suggest that the differences between ADHD and HC might be found in specific regions of interest (ROIs) [9], [19]. These studies demonstrated that the interactions between the local area of the brain and specific regions are more distinguishable between ADHD and HC. We therefore naturally ask, ''Is it good to cover all brain areas in diagnosing ADHD through a neural network model?'' Thus, we examined how to identify the important brain regions and how much these ROIs affect ADHD classification.

In this study, we intend to identify a specific answer to that question. The chosen dataset, evaluation method, and models are as follows. We combined all data sites as the training dataset to avoid biased results because the measurement parameters differ for each site. Then, we evaluated and compared the trained model using leave-one-site-out cross-validation (LOSO) [14] using the ROIs that we used for training. The separate channel CNN - RNN(SCCNN-RNN), which by Zhang et al. [14] proposed, is the model architecture for this experiment. Each model has the same number of trainable parameters, regardless of the number of ROIs. This means that we can control the variance of the result from the model capacity. Therefore, we can obtain a more accurate result related to the importance of the ROIs.

The experimental procedures were also designed to examine the existence of some critical areas in the identification of ADHD. With the SCCNN-RNN model, we examined the significance of the individual ROI using only one ROI feature for model training. Then, the ROIs were ranked according to the results. In the next step, we investigated how some of the ranked ROIs with a significant impact on the diagnosis of ADHD affect the classification accuracy. We discovered that using only the high-ranked ROIs rather than the entire ROIs is much better for classification. We also conducted experiments on three additional new architecture models based on SCCNN- RNN to supplement this result.

The contribution of our work can be summarized as follows: First, we demonstrated that different ROIs contribute differently to diagnosing ADHD, according to a deep learning experiment. This implies that one should investigate the significance of each ROI in ADHD diagnosis. Second, we demonstrated that in a deep learning experiment for ADHD, a diagnostic using a limited number of ROIs can perform better than a diagnostic using all ROIs. This indicates that diagnosing ADHD can be challenging considering all brain regions. Finally, we propose other deep learning architectures based on SCCNN – RNN.

In conclusion, even with a limited number of ROIs, the evaluation of the result demonstrated 70.6% accuracy. In Sections III and IV, we will explain the data selection process and a description of the experiment's models.

II. RELATED WORKS

A. BIOMARKER SELECTION IN fMRI FOR DISEASE DIAGNOSIS

In brain disease diagnosis, the brain's regional features from magnetic resonance are used importantly [20]. Among them, fMRI is used to understand the relationship between nerve activities in the special region of the brain and disease. Even though it is very complicated to figure out what characteristic is helpful to understand, there have been many efforts to reveal the connection.

The well-known approach is voxel-based feature extraction, which divides the brain into many small regions and obtains a characteristic in each area. Watanabe et al. [21] diagnosed Schizophrenia by learning the graphical features of 33 voxels. Moreover, Jin and Huang [22] used voxel-based feature extraction to diagnose depressive disorder.

However, there is a clear limit to diagnosing a disease using a voxel-based feature since it is obtained only by

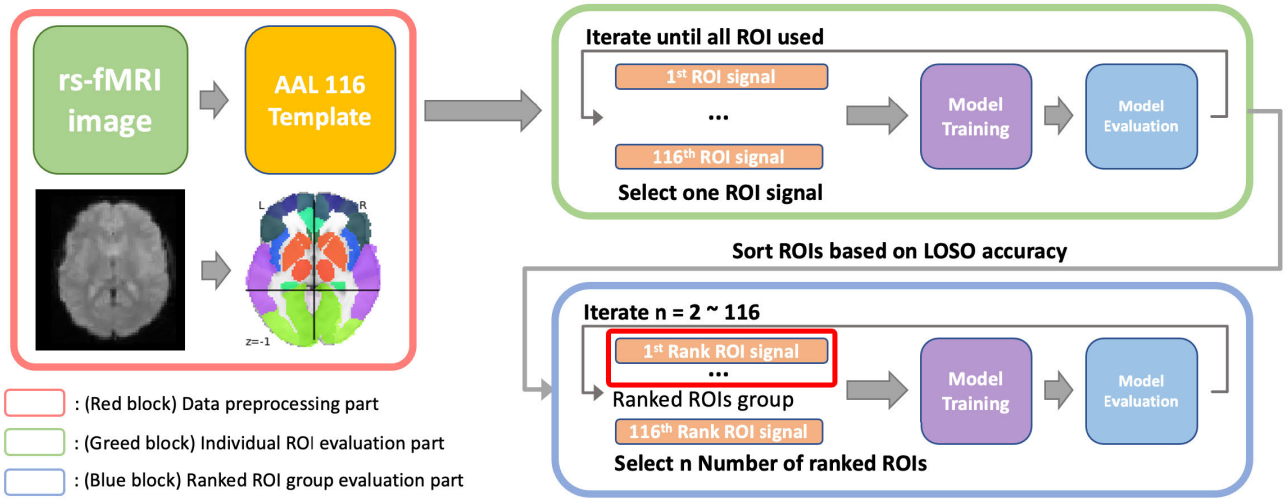

FIGURE 1. The overall pipeline of the proposed experiment procedure. The pipeline is divided into three parts. First, the red block is the data preprocessing part, which extracts the ROI features of rs-fMRI data preprocessed by the NIAK pipeline using an AAL 116 template. Second, the green block is the individual ROI evaluation part, which is used to identify the important ROIs using deep neural network models. Specifically, in this part, we train the model with only one ROI signal among 116 ROIs and evaluate the model using 'LOSO'. We evaluate all 116 ROIs independently. Third, the blue block is the ranked ROI group evaluation part, which selects the ranked n number of ROIs and evaluates the model.

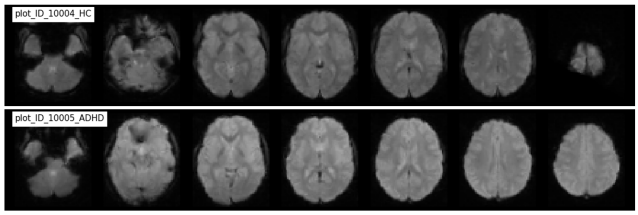

FIGURE 2. Comparison of ADHD-200's rs-fMRI image samples between HC subjects and ADHD patients preprocessed by NIAK template. The images are cut by several z-axis coordinates. (top) HC subject's rs-fMRI image at NYU site. (bottom) ADHD patient's rs-fMRI image at NYU site.

ROI Rank method

1: Prepare ROI-based rs-fMRI features in all site
2: Prepare ROI result list
3: **For** each ROI index
4: Select ROI features with one ROI index
5: Prepare site accuracy list
6: **For** each site
7: Prepare test set with ROI features of selected site samples
8: Prepare training set with ROI features of other site samples
9: Initialize the new NN model
10: Train the NN model with training set
11: Evaluate the model with test set
12: Append the accuracy in site accuracy list
13: **End for**
14: Calculate LOSO accuracy from site accuracy list
15: Append LOSO accuracy in ROI result list
16: **End for**
17: Rank with ROI result list in descending order
18: **Return** ROI indices from Ranked ROI result list

FIGURE 3. Pseudo-code of ROI rank method.

dividing the region of the brain without any medical information. To compensate for this limitation, ROI-based feature extraction where the region of the brain is divided by medical information is used. Dadi et al. [23] provided the performance of diagnosis when ROI-based features and machine learning are applied to various diseases.

In this work, we focus on the method to select a biomarker in ROI. Specifically, through the deep learning model, we evaluate the ability of each ROI to diagnose ADHD. Moreover, by using a deep learning model of ROIs, we study the relationship between the nerve activities in the special region of the brain and ADHD.

III. PROPOSED METHOD

A. NECESSITY OF CHECKING WHICH REGIONS OF THE BRAIN ARE IMPORTANT TO DIAGNOSE ADHD

As mentioned, several studies have been conducted to identify the biomarkers between HC and ADHD patients. Recently, deep neural network-based models have been used to study the biomarker, for which researchers used the entire brain.

However, findings suggested that the differences between ADHD and HC might be in specific or certain ROIs [9], [19]. Along these lines, we conducted a study to determine whether it is beneficial to examine all brain areas in diagnosing ADHD using a neural network model.

To answer this question, we designed the experiment shown in Fig 1, which shows the overall pipeline of the proposed experiment procedure. Our experiments were designed to determine how each ROI can be ranked and how using high-ranked ROIs can influence ADHD diagnosis. Because ranking each ROI is significantly difficult, we developed a method to rank each ROI. The developed method uses the AI model for each ROI, which is based on rs-fMRI data, to provide a score for ADHD diagnosis (For more detail, see

pseudo-code of ROI rank method in Fig 3). Then, as a feature subset selection [24], we investigated how many high-ranked ROIs can influence ADHD diagnosis. This study will enable us to answer the question raised above. Our experiments demonstrate that the SCCNN-RNN model using only a few ROIs provides 70.6% accuracy, which exceeds the existing results of 68.6% using all ROIs.

B. DATA SELECTION FOR THE EXPERIMENT

The rs-fMRI, shown in Fig 2, is a 4-dimensional structure that contains both spatial and temporal information about the brain. Therefore, the raw data obtained from a single subject contain many low-dimensional (x, y, z, t) features. This means that we require many data samples to learn a meaningful hidden feature of ADHD with a neural network. The neuro bureau [25] provides many data samples (∼1k) that are preprocessed using various methods (Athena, NIAK, Burner) used in the ADHD-200 Global competition. However, using them directly for the experiment presents some challenges. As previously stated, this is because there are still insufficient samples to directly use low-dimensional data for training.

Furthermore, the second reason regards the ADHD-200 Global competition dataset, which consists of several sites. In other words, different MRI device parameters were used to collect data from each fMRI site. The model will produce biased results depending on the initial setting of the measuring device if it is trained using fMRI data samples from a particular site.

To overcome these difficulties, we attempted to use as many data samples as possible in this study to obtain results independent of the measuring device. We constructed a training dataset from multiple sites together and extracted feature vectors that are less sensitive to the unique biological information (phenotype) and measure parameters. Handcraft feature extraction [26], [27] was frequently used in previous studies. However, these can vary depending on the context in which the fMRI data are collected. Therefore, this method is not appropriate for our situation. Therefore, we chose automated anatomical labeling (AAL 116) [28] for feature extraction.

Using the AAL 116 template, we anticipate that it will be possible to effectively extract features from low-dimensional fMRI data for the 116 ROIs. In summary, we chose the dataset from the five sites (NYU, Peking, OHSU, KKI, and NI) preprocessed by the NIAK pipeline [29] from the Neuro Bureau ADHD-200 preprocessed Repository (For more detail about preprocessing information, see [30].) We then extracted high-level features using the AAL template. These procedures enabled us to demonstrate that a specific ROI is useful for ADHD diagnosis in general fMRI data.

C. SEPARATE CHANNEL CNN - RNN ARCHITECTURE

As previously mentioned, we intend to identify the significant ROIs for diagnosing ADHD and HCs. To achieve this, we chose the SCCNN-RNN as the base model architecture for the experiment because it satisfies the following two criteria.

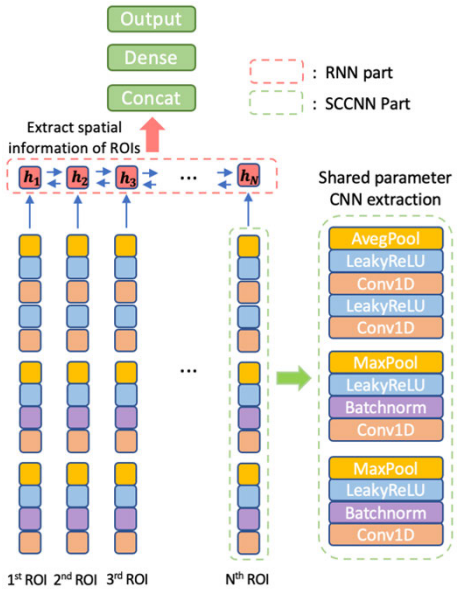

FIGURE 4. Architecture of the SCCNN - RNN. After passing the SCCNN part that extracts the bold signal of each ROI through convolution layers and the RNN part that learns the relationship between multiple ROIs, ADHD is determined from the output of the last step of RNN through two fully connected layers.

First, the SCCNN-RNN can extract spatial and temporal information from fMRI data. Particularly, SCCNN-RNN can be divided into two parts, each with a different purpose. First, the SCCNN part can extract the feature of the BOLD signal in each ROI using 1-D CNN. Because 1-D CNN performs well in signal processing, as shown in a recent study [31], it is used to handle fMRI data. Second, after processing ROI signals using a 1-D CNN, RNN can learn the dependence among ROIs and extract features about the relationship of ROIs.

Second, the SCCNN-RNN architecture can always maintain the same number of learnable weights regardless of changes in the input data dimension. For example, we trained several models using different ROIs and compared them with the evaluation results. If the input's shape changes the number of trainable parameters, the model's learning capacity can also be changed. This implies that we compared the influence of the ROI with inconsistent results. Therefore, to avoid this situation, we must control the trainable parameters.

Here, we describe the precise setting of the SCCNN-RNN for our experiments, as shown in Fig 4. In the SCCNN section, we stacked four layers using 1-D CNN. We used the 4-convolution layer. Each layer's channel number is 32, 64, 96, and 96, respectively. The stride size and the filter size were set to 1 and 3, respectively, as common parameters on the convolution layers. In the RNN section, we used the Bidirectional LSTM cell [32] because it has mechanisms whose performance has been demonstrated in many sequence data domains, such as speech recognition [33] and language model [34]. Additionally, we set the BiLSTM

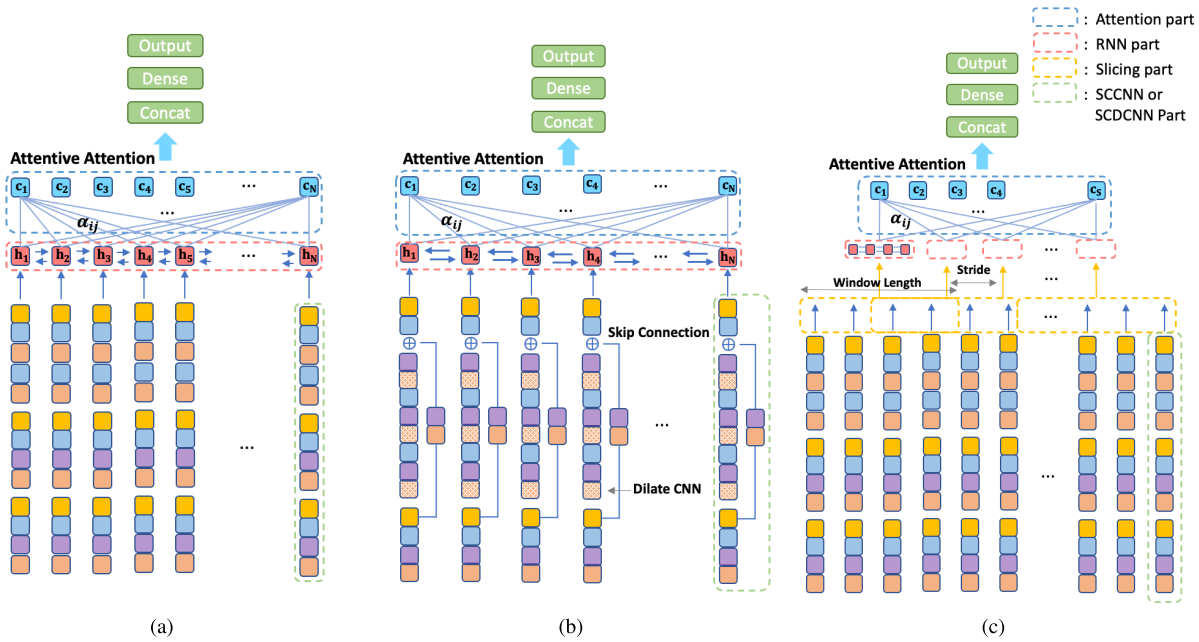

FIGURE 5. Differences in the proposed model architectures. (a) Separate Channel CNN - RNN with Attention (ASCRNN) (b) Separate Channel dilate CNN - RNN with Attention (ASDRNN) (c) Separate Channel CNN - slicing RNN with Attention (ASSRNN). All models contain the attention mechanism in common. In (a), only the attention mechanism from SCCNN - RNN structure is applied. In (b), the dilate CNN and skip connection on the SCCNN part based on the ASCRNN is applied. In (c), the slicing BiLSTM based on the ASCRNN is applied. ($c_i = \sum_{j=1}^{N_R} \alpha_{ij} h_j$: attention weight, h_j : output in j step on the RNN, R_N : number of ROIs used in training).

hidden state numbers to 128. Next, a fully connected layer with 128 neurons was connected to the output of the last T-step of the RNN. Finally, we applied the classification layer with a SoftMax activation to output the two-dimensional vectors as the probability of ADHD and HCs.

The SCCNN-RNN structure is a suitable and simple model to learn the spatial and temporal features from the rs-fMRI data for our experiment. However, it has an inefficient training structure. In the next section, we expand this structure to explore the more efficient result.

D. OTHER MODIFIED MODELS BASED ON THE SCCNN - RNN ARCHITECTURE

To develop the modified models from the SCCNN - RNN structure, we applied some concepts from the speech emotion recognition (SER) model [35], [36], [37]. We adopted concepts from the three different SER models. This is because SER using a neural network requires a structure for obtaining emotional information in a long sequence with a small amount of data. These share some of our problems. Therefore, we investigated the neural network structure to obtain features from fMRI data and various SCCNN-RNN-based model structures. Selecting and using a region with a high impact is more helpful in disease identification than using all regions.

As shown in Fig 5, these three SCCNN-RNN modified models show slight differences. However, the attention mechanism is frequently applied. The attention mechanism typically improves model performance if the training data are sequential. In the SCCNN-RNN structure, the attention mechanism only uses the last hidden state outputs from BiLSTM as the next layer's inputs. Therefore, learning the significance of ROIs is structurally difficult. To overcome this challenge, we designed the attention mechanism to focus on the significant ROI with hidden states at all times step.

The attention mechanism has been used in several ways recently [38], [39], [40]. In our study, we chose an attentive attention method [14]. Particularly, to learn the correlation between the two reference ROIs, after linear transformation of the comparison vector with a learnable weight matrix, mapping into a non-linear function was considered. In this study, despite using the same method as the previous study, there are differences. In [14], the attention was stacked after the SCCNN part, but we stacked the SCCNN part, RNN part, and attentive attention in that order. The attention method was applied in this manner to consider not only relationships between two areas but also relationships between several areas. For example, $\boldsymbol{h}_j$ of jth BiLSTM's hidden state consists of the forward hidden state $\overrightarrow{\boldsymbol{h}}_j$, containing information from the first ROI to the jth ROI, and backward hidden state $\overleftarrow{\boldsymbol{h}}_j$, containing information from the R_Nth ROI to the jth ROI in reverse order. Additionally, we learnt the correlation α_{ij} between $\boldsymbol{h}_i$ and $\boldsymbol{h}_j$ using the attention layer. Therefore, all ROIs that we chose can be considered in one step. Equations (1), (2) and (3) describe the process. This model is called

an ASCRNN. This attention was also applied to the two models proposed later.

$$\boldsymbol{h}_j = \text{Concat}\left(\vec{\boldsymbol{h}}_j, \overleftarrow{\boldsymbol{h}}_j\right), \quad 1 \le j \le N_R. \tag{1}$$

$$\alpha_{ij} = \text{attentive}\left(\boldsymbol{h}_i, \boldsymbol{h}_j\right) \tag{2}$$

$$\boldsymbol{c}_i = \sum_{j=1}^{N_R} \alpha_{ij} \boldsymbol{h}_j \tag{3}$$

The next-modified model called ASDRNN focused on the BOLD signal extraction. This model differs from the SCCNN section. According to a previous study [16], learning with only the relationship within a specific frame of the BOLD signal is helpful in ADHD diagnosis. Therefore, we replaced the 1-D CNN with a dilation 1-D CNN [41]. Additionally, to address the gradient vanishing problem of deep neural networks, we applied a skip connection [42] after the final batch normalization layer. The skip connection structure adds elements between the feature values of the previous present layers. This provides a smooth gradient flow. So it is called a separate channel dilate CNN (SCDCNN) with skip connection. The detailed structure of SCDCNN is shown in Fig 5(b) and 6. The dilate rate was set to 2 in dilation 1-D CNN.

Fig 5(c) shows the last modified model named ASSRNN. This model uses a segmented area as input to the RNN rather than the entire ROI area to obtain the relationship between partitioned regions. To achieve this, we applied the slicing BiLSTM [37] rather than the BiLSTM in the ASCRNN model. The slicing BiLSTM's inputs ($X^{(l)}$) are a set of subsequences splatted from the original ROI feature sequences ($\boldsymbol{x}_i$: ith ROI's SCCNN output feature vector) with a constant window size (w) and stride size (s). This can be expected to focus on the relationship within the small number of ROIs and prevent the gradient vanishing problem from occurring as the RNN structure's time step lengthens. This process is expressed in (4), (5) and (6).

$$l = 1, 2, 3, \ldots, \lceil \frac{N_R - w}{s} + 1 \rceil \tag{4}$$

$$X^{(l)} = \begin{cases} \left[\boldsymbol{x}_{N_R-w+1}, \ldots, \boldsymbol{x}_{N_R}\right], & l = \lceil \frac{N_R-w}{s} + 1 \rceil \\ \left[\boldsymbol{x}_{1+(l-1)s}, \ldots, \boldsymbol{x}_{w+(l-1)s}\right], & \text{elsewhere} \end{cases} \tag{5}$$

$$H^{(l)} = \text{BiLSTM}\left(X^{(l)}\right) \tag{6}$$

IV. EXPERIMENT AND RESULT

A. SETTINGS FOR MODEL TRAINING AND EVALUATION

To analyze the ROI selection results, all hyperparameters required for learning were identical in our experiments. The hyperparameter setting was based on the experimental results. Particularly, we used the Adam optimizer [43]. A learning rate was chosen with 1e-4. Xavier initialization [44] was used as the initialization method for all trainable weights. Additionally, to prevent the overfitting problem, we used l2 regularization with a factor of 0.0005. The leaky ReLU [45] with a 0.1 slope coefficient was chosen as the activation function. Next, to avoid bias owing to an imbalanced dataset corresponding to ADHD and HC, the same number of each class (ADHD, HC) was sampled for each mini-batch. The mini-batch size was set to 32. We then set the binary cross-entropy for the loss function. For the evaluation metric, LOSO accuracy [14] was chosen for evaluating the model. LOSO is a type of cross-validation that splits the data in each site. Because we use 5 different sites, 5 site fold evaluation was done in one experiment. Therefore, the dependent characteristics (parameters of the fMRI measurement device in each site) could be avoided by proceeding with the evaluation using the dataset from another site not used for model training. The experiment results for the ROIs that play an essential role in diagnosis can be generalized. For more detail about the experiment setting, see in GitHub site at https://github.com/byunggunkim/Finding-Essential-Parts-in-brain

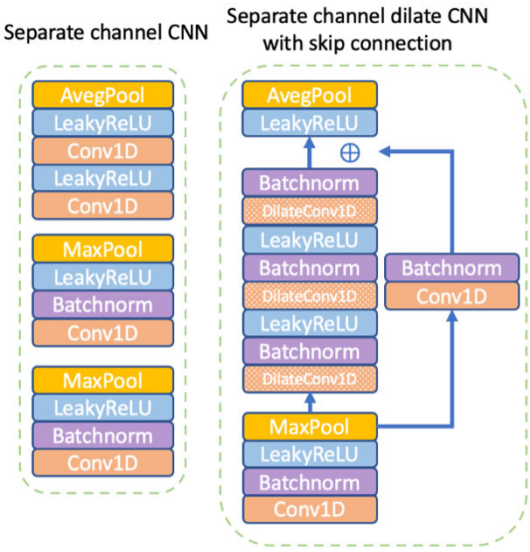

FIGURE 6. Contrast between SCCNN and SCDCNN with skip connection architectures.

TABLE 1. The data composition of each site that we used in our experiments.

	NYU	Peking	OHSU	KKI	NI	Total
ADHD	147	101	43	25	36	352
HC	110	143	70	69	37	429
Total	257	244	133	94	73	781
Ratio of ADHD	0.57	0.41	0.38	0.27	0.49	0.45

B. DETAIL OF THE DATASET COMPOSITION

For this experiment, we used rs-fMRI data samples from the ADHD-200 competition [25]. They consist of data from eight institutions (NYU: New York University child study center, Peking: Peking University, OHSU: Oregon Health

TABLE 2. The ranking of ROIs in AAL 116 template based on SCCNN-RNN model.

Rank	ROI name	Rank	ROI name	Rank	ROI name	Rank	ROI name
1	Rectus_R	30	Caudate_L	59	Occipital_Mid_L	88	Thalamus_L
2	Postcentral_R	31	Frontal_Inf_Orb_L	60	Vermis_7	89	Fusiform_L
3	Olfactory_L	32	Cerebelum_Crus2_R	61	Caudate_R	90	Precentral_R
4	Rectus_L	33	Heschl_R	62	Cerebelum_7b_R	91	Occipital_Inf_L
5	Frontal_Sup_Orb_R	34	Frontal_Sup_Orb_L	63	Cerebelum_4_5_L	92	Lingual_R
6	Olfactory_R	35	Frontal_Sup_Medial_R	64	Occipital_Inf_R	93	Precentral_L
7	ParaHippocampal_R	36	Paracentral_Lobule_L	65	Cingulum_Mid_R	94	Frontal_Inf_Oper_R
8	Frontal_Sup_R	37	Cerebelum_7b_L	66	Parietal_Sup_L	95	Supp_Motor_Area_L
9	Frontal_Mid_L	38	Cerebelum_3_R	67	Cuneus_R	96	Cerebelum_Crus1_R
10	Cingulum_Ant_L	39	Parietal_Sup_R	68	Supp_Motor_Area_R	97	Paracentral_Lobule_R
11	Pallidum_L	40	Temporal_Pole_Mid_L	69	Vermis_1_2	98	Hippocampus_R
12	Frontal_Med_Orb_R	41	Cerebelum_6_R	70	Postcentral_L	99	Temporal_Mid_R
13	ParaHippocampal_L	42	Cerebelum_8_R	71	Parietal_Inf_R	100	Cerebelum_9_L
14	Vermis_9	43	Cingulum_Post_R	72	Rolandic_Oper_R	101	Occipital_Sup_R
15	Frontal_Med_Orb_L	44	Angular_L	73	Parietal_Inf_L	102	Vermis_10
16	Frontal_Inf_Orb_R	45	Vermis_8	74	Frontal_Sup_Medial_L	103	Precuneus_L
17	Frontal_Mid_Orb_R	46	Frontal_Sup_L	75	Amygdala_L	104	Frontal_Mid_Orb_L
18	Temporal_Mid_L	47	Vermis_4_5	76	Occipital_Mid_R	105	Temporal_Sup_R
19	Cerebelum_Crus2_L	48	Pallidum_R	77	SupraMarginal_R	106	Frontal_Inf_Oper_L
20	Temporal_Pole_Sup_L	49	Vermis_6	78	Calcarine_R	107	Cerebelum_10_L
21	Cuneus_L	50	Precuneus_R	79	SupraMarginal_L	108	Frontal_Inf_Tri_L
22	Putamen_L	51	Temporal_Inf_R	80	Putamen_R	109	Vermis_3
23	Cingulum_Ant_R	52	Cerebelum_6_L	81	Cerebelum_8_L	110	Cerebelum_9_R
24	Cingulum_Mid_L	53	Frontal_Inf_Tri_R	82	Cingulum_Post_L	111	Calcarine_L
25	Heschl_L	54	Lingual_L	83	Temporal_Inf_L	112	Cerebelum_3_L
26	Insula_R	55	Frontal_Mid_R	84	Hippocampus_L	113	Fusiform_R
27	Amygdala_R	56	Temporal_Sup_L	85	Insula_L	114	Cerebelum_4_5_R
28	Temporal_Pole_Sup_R	57	Cerebelum_Crus1_L	86	Temporal_Pole_Mid_R	115	Occipital_Sup_L
29	Angular_R	58	Rolandic_Oper_L	87	Cerebelum_10_R	116	Thalamus_R

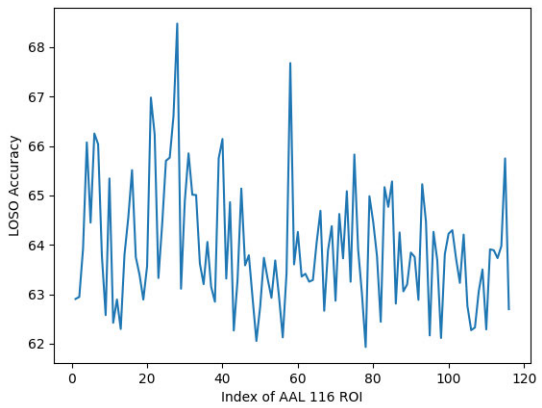

FIGURE 7. Accuracy according to individual ROI when we trained the SCCNN-RNN with only one individual ROI.

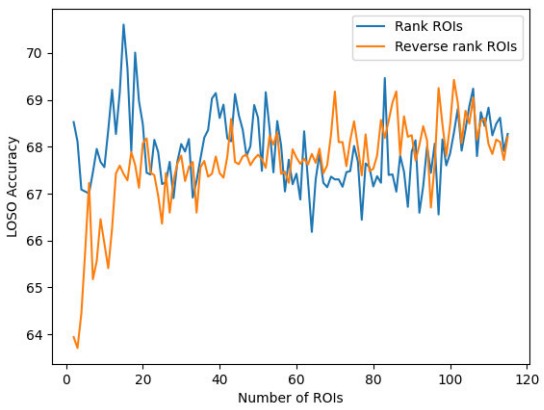

FIGURE 8. The accuracy when training the SCCNN-RNN as we increase the number of learning ROIs. (blue line) The accuracy in the learning scenario when selecting in order of ROIs with the highest rank. (orange line) The accuracy in the learning scenario when selecting in order of ROI with the lowest rank.

Sciences University, KKI: Kennedy Krieger Institute, NI: NeuroIMAGE, BHBU: Bradley/Brown University, and Pitt: University of Pittsburgh, WUSTL: Washington University at Saint Louis). BHBU, Pitt, and WUSTL are difficult to use for supervised learning; therefore, five other sites (NYU, Peking, OHSU, KKI, and NI) are used. Moreover, to compensate for the lack of data, all data samples from each site were combined and considered as a single dataset. For example, if we use the NYU site as a test set, the other site's (Peking, OHSU, KKI, NI) data samples are used for training. The overall structure of the data composition is shown in Table 1.

C. SELECTING AN IMPORTANT REGION OF THE BRAIN ACCORDING TO AAL 116 ROIS USING SCCNN-RNN

To determine the significance of individual ROIs for ADHD discrimination, we evaluated the accuracy using an independent neural network model trained with a specific ROI. For this experiment, we used LSTM-based SCCNN-RNN models. Fig 7 shows the diagnosis accuracy trained with a specific ROI. The experiment's accuracy data had a wide range of distributions (minimum accuracy: 61.93% with

TABLE 3. Comparison of accuracy in ADHD-200 classification models using AAL template.

Proposed paper	Model name	Used site name list	Overall accuracy with all ROIs	LOSO accuracy with specific ROIs (Number of ROIs used in the experiment)
[12]	FCNet	NYU, Peking, NI	60.4	-
[13]	DeepfMRI	NYU, Peking, NI	67.9	-
[14]	SCCNN - Attention	NYU, Peking, OHSU, KKI, NI	68.6	-
[14]	SCCNN - RNN	NYU, Peking, OHSU, KKI, NI	63.6	70.60 (15)
-	ASCRNN	NYU, Peking, OHSU, KKI, NI	65.20	69.97 (20)
-	ASDRNN	NYU, Peking, OHSU, KKI, NI	68.40	68.05 (17)
-	ASSRNN	NYU, Peking, OHSU, KKI, NI	66.86	70.46 (13)

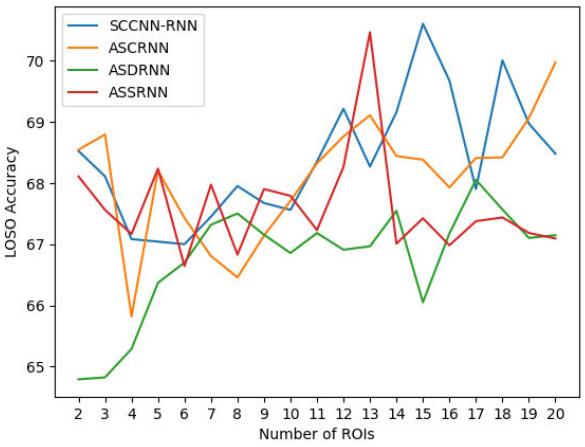

FIGURE 9. Accuracy when training the other modified models (ASCRNN, ASDRNN, ASSRNN) as the number of ROIs based on the rank order increases.

index=77, minimum accuracy: 68.47% with index=28). This indicates a significant result when learning with only one ROI because it has fewer fMRI features than all other ROIs. It can be expected that there may be a region that plays an essential role in discriminating ADHD. The high-ranked ROIs' (up to 20) brain map can be seen in Fig 10. Based on these results, we will show how learning by selecting a few significant ROIs differs from using all ROIs, in the following experiment.

D. ACCURACY ANALYSIS FOR ADHD DISCRIMINATION ACCORDING TO ROI RANKING IN SCCNN-RNN

The experiment was performed to determine how the association between significant ROIs can be understood in ADHD discrimination. The specific progress of the experiment is as follows. According to the ROI ranking from Section IV-C, the regions at the top were selected sequentially, and the number of ROI features gradually increased. Additionally, the experiment was conducted using independent neural network models. Furthermore, the same model (SCCNN-RNN) was used to reduce the difference that will appear owing to the neural network model's parameters changing as the input data size increased.

Fig 8 shows the model's accuracy trained with ranking ROIs. From the blue line in Fig 8, we can observe the following. First, high accuracy is obtained when learning by selecting ROIs in a particular order, where the learning is performed by selecting ROIs in the order obtained. Some ROIs play a significant role in the diagnosis. As shown in Fig 8, using the ROI in the top 20 results in a ranking that achieves high accuracy. An accuracy of 70.6% was obtained when ROI up to the 15th rank was used for training. Second, it becomes difficult to identify areas that yield better results than before as the ROI used for learning increases. This means that using many ROIs can be a hindrance to ADHD diagnosis. This demonstrates how, even with very little data, selecting the right input features can be crucial.

Fig 8 also shows the results of selecting the ROI in reverse order, as shown by the orange line. As expected, the case of reverse order shows the opposite result compared with the case of high ranking. Relatively low accuracy is obtained when using up to the 20th rank of the reverse ranks, but the accuracy tends to increase as more ROIs are gradually used. This implies that learning with ROIs of low importance as determined by accuracy does not help much with the diagnosis, but it might be helpful if the number of ROIs used for subsequent learning increases. That is, high-rank ROIs complement low-rank ROIs.

Our experiments demonstrate that selecting significant ROIs is necessary for diagnosing ADHD when SC-CNN–RNN is used as an AI model. Therefore, it is natural to ask whether the results can be confirmed in different AI models that are considered variants of the SCCNN – RNN.

E. ACCURACY ANALYSIS FOR ADHD DISCRIMINATION ACCORDING TO ROI RANKING IN MODIFIED MODELS

To investigate the impact on the significance of ROI, we performed experiments with other modified models (ASCRNN, ASDRNN, and ASSRNN) mentioned in Section III-D. A detailed description of the models can be found in the previous section. The experiment was performed according to the procedures described in Section IV-D. However, the ROI used for learning only reached the 20th rank. Because Fig 8 indicates that using 20 significant ROIs provides the best result, we checked whether the variants of our AI model can provide similar results.

Fig 9 and Table 3 allow us to describe the result. First, learning with ROIs selected according to their rank should yield better results than learning with all ROIs. Furthermore,

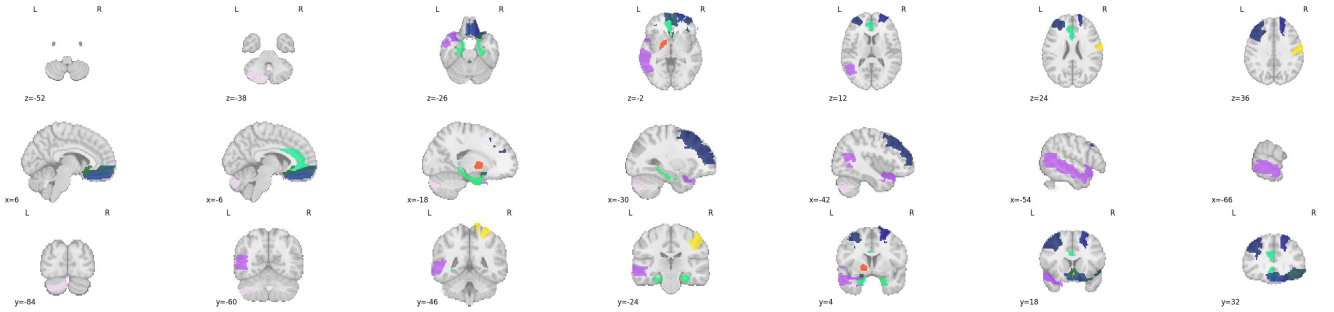

FIGURE 10. Brain map of the selected region with the 20th ranked ROI in AAL 116 atlas based on SCCNN-RNN model.

TABLE 4. Each site accuracy of different SCCNN-type models with ranked ROIs.

Model name	NYU	Peking	OHSU	KKI	NI	LOSO
SCCNN - RNN	68.09	63.93	72.57	74.47	73.97	70.6
ASCRNN	64.59	64.75	73.45	74.47	72.60	69.97
ASDRNN	59.14	62.29	69.02	74.47	75.34	68.05
ASSRNN	64.59	64.34	69.03	77.66	76.71	70.46

all models provided accuracies that are between 68% and 70% despite using fewer areas than all 116 areas. For SCCNN-RNN and ASSRNN, the accuracies of 70.6% (15) and 70.46% (13) were obtained, respectively, which exceeded 70% accuracy (Table 3). This result is 2% higher than the previous result (68.6%). Second, the modified models based on SCCNN-RNN have between 10 and 20 ROIs that provide good accuracy (Fig 9). This is slightly different from the case where only a few areas (for example 1-5 rank ROI) are used. Therefore, one should use several significant ROIs.

Some models shown in Fig 9 performed better when the entire ROIs were used than a few significant ROIs. This occurred because of underfitting owing to a lack of ADHD data. In the case of ASDRNN, the complexity of the model causes this phenomenon.

To summarize, a specific part of the brain must be used to improve the diagnosis. The simplest model (SCCNN - RNN) produced the best accuracy. There was an improvement of approximately 7% when higher-ranking ROIs were used. Therefore, finding the ROI, which plays a significant role in diagnosing ADHD, is necessary when using AI to treat ADHD.

V. DISCUSSION AND LIMITATION

In this work, we wanted to check whether the deep-learning model can find the characteristics for diagnosing ADHD. In this work, we found that using not all but some ROIs is more effective in diagnosing ADHD. Here, we want to add remarks about our findings.

First, it is about ROIs, ranked by our deep learning models. It should be emphasized that the importance of each ROI is not evaluated by medical knowledge. Therefore, it is meaningful to know the relationship between high-ranked ROIs and known medical knowledge. For this purpose, let us discuss the medical meaning of 20-high ranked ROIs. 7 ROIs among 20 ranked ROIs belong to the frontal of the brain. Those ROIs consist of 39% of the frontal region. This fact supports the medical investigation that a relationship exists between the Frontal lobe and ADHD. Since the frontal lobe plays a role in concentration, the malfunction of a frontal region may cause ADHD. Therefore, in future research, we will provide a detailed study of the relationship between ROIs of a frontal region and ADHD, using deep-learning models.

The second is about the difference in the considered sites. As shown in Table 4, the accuracy in each site differs hugely (Standard deviation of SCCNN-RNN site accuracy in Table 4: 4.5).

For instance, we used the Neuro Bureau ADHD-200 preprocessed repository [25], data provided for deep-learning researchers. The data consists of various sites, each using different parameters to obtain fMRI data.

This repository also contains fMRI data, which is pre-processed by various methods such as (Athena, Burner, NIAK). Therefore, even though one uses the data with the same preprocessing method, there can be a possibility to obtain different results because the detailed parameters in the preprocessing method can differ [47]. Also, the data results obtained from the different preprocessing methods can differ.

Therefore, for a precise result, one needs to investigate the experiment using data from many different preprocessing methods in rs-fMRI not only Athena, Burner but also CCS [48], CPAC [49], and DPARSF [50].

VI. CONCLUSION

To diagnose ADHD, rs-fMRI data are frequently used because they contain much information about the brain. In this study, we demonstrated that identifying ROI that provides important areas in the brain can help diagnose ADHD. Moreover, it was found that using only 15 ROIs in the ranking order can significantly improve performance (70.6%) than using all areas for the diagnosis. This implies that establishing appropriate criteria for the ROI's significance can result in an accurate diagnosis.

However, The medical biomarker that distinguishes between ADHD and normal is still elusive. Among many causes, one thing is the limitation of medical data related to ADHD. To accurately diagnose ADHD, more ADHD data are needed. Fortunately, nowadays, an open platform like openneuro containing large amounts of data is available (see https://openneuro.org/ (accessed on 19 October, 2022)).

It is known that Autism spectrum disorder (ASD) may have a close relation with ADHD [51], [52]. Therefore, it is significant to apply our approach by selecting important ROIs and building a deep-learning model based on the result to diagnose Autism spectrum disorder (ASD). Also, it is interesting to find a unified model to diagnose both ASD and ADHD.

REFERENCES

[1] R. A. Barkley, "Behavioral inhibition, sustained attention, and executive functions: Constructing a unifying theory of ADHD," *Psychol. Bull.*, vol. 121, no. 1, pp. 65–94, Jan. 1997.

[2] S. V. Faraone, J. Sergeant, C. Gillberg, and J. Biederman, "The worldwide prevalence of ADHD: Is it an American condition?" *World Psychiatry*, vol. 2, no. 2, p. 104, 2003.

[3] G. Polanczyk, M. S. de Lima, B. L. Horta, J. Biederman, and L. A. Rohde, "The worldwide prevalence of ADHD: A systematic review and metaregression analysis," *Amer. J. Psychiatry*, vol. 164, no. 6, pp. 942–948, Jun. 2007.

[4] B. T. Felt, B. Biermann, J. G. Christner, P. Kochhar, and R. Van Harrison, "Diagnosis and management of ADHD in children," *Amer. Family Physician*, vol. 90, no. 7, pp. 456–464, 2014.

[5] M. Greicius, "Resting-state functional connectivity in neuropsychiatric disorders," *Current Opinion Neurol.*, vol. 21, no. 4, pp. 424–430, 2008.

[6] C.-Z. Zhu, Y.-F. Zang, Q.-J. Cao, C.-G. Yan, Y. He, T.-Z. Jiang, M.-Q. Sui, and Y.-F. Wang, "Fisher discriminative analysis of resting-state brain function for attention-deficit/hyperactivity disorder," *NeuroImage*, vol. 40, no. 1, pp. 110–120, Mar. 2008.

[7] S. Dey, A. R. Rao, and M. Shah, "Attributed graph distance measure for automatic detection of attention deficit hyperactive disordered subjects," *Frontiers Neural Circuits*, vol. 8, p. 64, Jun. 2014.

[8] X. Guo, X. An, D. Kuang, Y. Zhao, and L. He, "ADHD-200 classification based on social network method," in *Proc. Int. Conf. Intell. Comput.* Cham, Switzerland: Springer, 2014, pp. 233–240.

[9] P. Lin, J. Sun, G. Yu, Y. Wu, Y. Yang, M. Liang, and X. Liu, "Global and local brain network reorganization in attention-deficit/hyperactivity disorder," *Brain Imag. Behav.*, vol. 8, no. 4, pp. 558–569, Dec. 2014.

[10] B. Sen, N. C. Borle, R. Greiner, and M. R. G. Brown, "A general prediction model for the detection of ADHD and autism using structural and functional MRI," *PLoS ONE*, vol. 13, no. 4, Apr. 2018, Art. no. e0194856.

[11] Y. Tang, C. Wang, Y. Chen, N. Sun, A. Jiang, and Z. Wang, "Identifying ADHD individuals from resting-state functional connectivity using subspace clustering and binary hypothesis testing," *J. Attention Disorders*, vol. 25, no. 5, pp. 736–748, Mar. 2021.

[12] A. Riaz, M. Asad, S. M. R. Al-Arif, E. Alonso, D. Dima, P. Corr, and G. Slabaugh, "FCNet: A convolutional neural network for calculating functional connectivity from functional MRI," in *Proc. Int. Workshop Connectomics Neuroimaging* Cham, Switzerland: Springer, 2017, pp. 70–78.

[13] A. Riaz, M. Asad, S. M. M. R. A. Arif, E. Alonso, D. Dima, P. Corr, and G. Slabaugh, "Deep fMRI: AN end-to-end deep network for classification of fMRI data," in *Proc. IEEE 15th Int. Symp. Biomed. Imag. (ISBI)*, Apr. 2018, pp. 1419–1422.

[14] T. Zhang, C. Li, P. Li, Y. Peng, X. Kang, C. Jiang, F. Li, X. Zhu, D. Yao, B. Biswal, and P. Xu, "Separated channel attention convolutional neural network (SC-CNN-attention) to identify ADHD in multi-site rs-fMRI dataset," *Entropy*, vol. 22, no. 8, p. 893, Aug. 2020.

[15] L. Zou, J. Zheng, C. Miao, M. J. Mckeown, and Z. J. Wang, "3D CNN based automatic diagnosis of attention deficit hyperactivity disorder using functional and structural MRI," *IEEE Access*, vol. 5, pp. 23626–23636, 2017.

[16] Z. Mao, Y. Su, G. Xu, X. Wang, Y. Huang, W. Yue, L. Sun, and N. Xiong, "Spatio-temporal deep learning method for ADHD fMRI classification," *Inf. Sci.*, vol. 499, pp. 1–11, Oct. 2019.

[17] Y. Zhang, Z. Wang, J. Zhang, C. Wang, Y. Wang, H. Chen, L. Shan, J. Huo, J. Gu, and X. Ma, "Deep learning model for classifying endometrial lesions," *J. Translational Med.*, vol. 19, no. 1, pp. 1–13, Dec. 2021.

[18] A. Bilal, G. Sun, S. Mazhar, A. Imran, and J. Latif, "A transfer learning and U-Net-based automatic detection of diabetic retinopathy from fundus images," *Comput. Methods Biomechanics Biomed. Eng., Imag. Visualizat.*, vol. 10, no. 6, pp. 663–674, Nov. 2022.

[19] A. Eloyan, J. Muschelli, M. B. Nebel, H. Liu, F. Han, T. Zhao, A. D. Barber, S. Joel, J. J. Pekar, S. H. Mostofsky, and B. Caffo, "Automated diagnoses of attention deficit hyperactive disorder using magnetic resonance imaging," *Frontiers Syst. Neurosci.*, vol. 6, p. 61, Aug. 2012.

[20] M. Liu, J. Zhang, D. Nie, P.-T. Yap, and D. Shen, "Anatomical landmark based deep feature representation for MR images in brain disease diagnosis," *IEEE J. Biomed. Health Informat.*, vol. 22, no. 5, pp. 1476–1485, Sep. 2018.

[21] T. Watanabe, D. Kessler, C. Scott, M. Angstadt, and C. Sripada, "Disease prediction based on functional connectomes using a scalable and spatially-informed support vector machine," *NeuroImage*, vol. 96, pp. 183–202, Aug. 2014.

[22] J. Jin and L. Huang, "A region-based feature extraction method for rs-fMRI of depressive disorder classification," in *Proc. Int. Conf. Comput. Vis., Image Deep Learn. (CVIDL)*, Jul. 2020, pp. 707–710.

[23] K. Dadi, M. Rahim, A. Abraham, D. Chyzhyk, M. Milham, B. Thirion, and G. Varoquaux, "Benchmarking functional connectome-based predictive models for resting-state fMRI," *NeuroImage*, vol. 192, pp. 115–134, May 2019.

[24] M. A. Hall and L. A. Smith, "Practical feature subset selection for machine learning," in *Proc. 21st Australas. Comput. Sci. Conf. Comput. Sci. (ACSC)*, Perth, WA, Australia, C. McDonald, Ed. Berlin, Germany: Springer, Feb. 1998, pp. 181–191. 4-6 February, 1998(pp. 181-191).

[25] P. Bellec, C. Chu, F. Chouinard-Decorte, Y. Benhajali, D. S. Margulies, and R. C. Craddock, "The neuro bureau ADHD-200 preprocessed repository," *NeuroImage*, vol. 144, pp. 275–286, Jan. 2017.

[26] M. R. G. Brown, G. S. Sidhu, R. Greiner, N. Asgarian, M. Bastani, P. H. Silverstone, A. J. Greenshaw, and S. M. Dursun, "ADHD-200 global competition: Diagnosing ADHD using personal characteristic data can outperform resting state fMRI measurements," *Frontiers Syst. Neurosci.*, vol. 6, p. 69, Sep. 2012.

[27] D. Dai, J. Wang, J. Hua, and H. He, "Classification of ADHD children through multimodal magnetic resonance imaging," *Frontiers Syst. Neurosci.*, vol. 6, p. 63, Sep. 2012.

[28] N. Tzourio-Mazoyer, B. Landeau, D. Papathanassiou, F. Crivello, O. Etard, N. Delcroix, B. Mazoyer, and M. Joliot, "Automated anatomical labeling of activations in SPM using a macroscopic anatomical parcellation of the MNI MRI single-subject brain," *NeuroImage*, vol. 15, no. 1, pp. 273–289, Jan. 2002.

[29] S. Lavoie-Courchesne, P. Rioux, F. Chouinard-Decorte, T. Sherif, M.-E. Rousseau, S. Das, R. Adalat, J. Doyon, C. Craddock, D. Margulies, C. Chu, O. Lyttelton, A. C. Evans, and P. Bellec, "Integration of a neuroimaging processing pipeline into a pan-Canadian computing grid," *J. Phys., Conf.*, vol. 341, Feb. 2012, Art. no. 012032.

[30] *Neurobureau NIAK Pipeline*. Accessed: Jul. 3, 2023. [Online]. Available: https://www.nitrc.org/plugins/mwiki/index.php?title=neurobureau: NIAK

[31] S. Kiranyaz, T. Ince, O. Abdeljaber, O. Avci, and M. Gabbouj, "1-D convolutional neural networks for signal processing applications," in *Proc. IEEE Int. Conf. Acoust., Speech Signal Process. (ICASSP)*, May 2019, pp. 8360–8364.

[32] A. Graves and J. Schmidhuber, "Framewise phoneme classification with bidirectional LSTM and other neural network architectures," *Neural Netw.*, vol. 18, nos. 5–6, pp. 602–610, Jul. 2005.

[33] A. Graves, A.-R. Mohamed, and G. Hinton, "Speech recognition with deep recurrent neural networks," in *Proc. IEEE Int. Conf. Acoust., Speech Signal Process.*, May 2013, pp. 6645–6649.

[34] M. Sundermeyer, R. Schlüter, and H. Ney, "LSTM neural networks for language modeling," in *Proc. 13th Annu. Conf. Int. Speech Commun. Assoc.*, 2012, pp. 1–4.

[35] H. Meng, T. Yan, F. Yuan, and H. Wei, "Speech emotion recognition from 3D Log-Mel spectrograms with deep learning network," *IEEE Access*, vol. 7, pp. 125868–125881, 2019.

[36] Y. Xie, R. Liang, Z. Liang, C. Huang, C. Zou, and B. Schuller, "Speech emotion classification using attention-based LSTM," *IEEE/ACM Trans. Audio, Speech, Language Process.*, vol. 27, no. 11, pp. 1675–1685, Nov. 2019.

[37] Z. Peng, X. Li, Z. Zhu, M. Unoki, J. Dang, and M. Akagi, "Speech emotion recognition using 3D convolutions and attention-based sliding recurrent networks with auditory front-ends," *IEEE Access*, vol. 8, pp. 16560–16572, 2020.
[38] D. Bahdanau, K. Cho, and Y. Bengio, "Neural machine translation by jointly learning to align and translate," 2014, *arXiv:1409.0473*.
[39] M.-T. Luong, H. Pham, and C. D. Manning, "Effective approaches to attention-based neural machine translation," 2015, *arXiv:1508.04025*.
[40] A. Vaswani, N. Shazeer, N. Parmar, J. Uszkoreit, L. Jones, A. N. Gomez, Ł. Kaiser, and I. Polosukhin, "Attention is all you need," in *Proc. Adv. Neural Inf. Process. Syst.*, 2017, pp. 5998–6008.
[41] F. Yu and V. Koltun, "Multi-scale context aggregation by dilated convolutions," 2015, *arXiv:1511.07122*.
[42] K. He, X. Zhang, S. Ren, and J. Sun, "Deep residual learning for image recognition," in *Proc. IEEE Conf. Comput. Vis. Pattern Recognit. (CVPR)*, Jun. 2016, pp. 770–778.
[43] D. P. Kingma and J. Ba, "Adam: A method for stochastic optimization," 2014, *arXiv:1412.6980*.
[44] X. Glorot and Y. Bengio, "Understanding the difficulty of training deep feedforward neural networks," in *Proc. 13th Int. Conf. Artif. Intell. Statist.*, 2010, pp. 249–256.
[45] A. L. Maas, A. Y. Hannun, and A. Y. Ng, "Rectifier nonlinearities improve neural network acoustic models," in *Proc. ICML*, 2013, pp. 1–3.
[46] G. M. Grodzinsky and R. Diamond, "Frontal lobe functioning in boys with attention-deficit hyperactivity disorder," *Develop. Neuropsychol.*, vol. 8, no. 4, pp. 427–445, Jan. 1992.
[47] T. Glatard, L. B. Lewis, R. F. da Silva, R. Adalat, N. Beck, C. Lepage, P. Rioux, M.-E. Rousseau, T. Sherif, E. Deelman, N. Khalili-Mahani, and A. C. Evans, "Reproducibility of neuroimaging analyses across operating systems," *Frontiers Neuroinform.*, vol. 9, p. 12, Apr. 2015.
[48] T. Xu, Z. Yang, L. Jiang, X.-X. Xing, and X.-N. Zuo, "A connectome computation system for discovery science of brain," *Sci. Bull.*, vol. 60, no. 1, pp. 86–95, Jan. 2015.
[49] C. Craddock, S. Sikka, B. Cheung, R. Khanuja, S. S. Ghosh, C. Yan, Q. Li, D. Lurie, J. Vogelstein, and R. Burns, "Towards automated analysis of connectomes: The configurable pipeline for the analysis of connectomes (C-PAC)," *Front Neuroinform*, vol. 7, no. 1, pp. 57–72, Jul. 2013.
[50] *Data Processing Assistant for Resting-State fMRI (DPARSF)*. Accessed: Oct. 16, 2023. [Online]. Available: http://www.rfmri.org/DPARSF
[51] T. Stevens, L. Peng, and L. Barnard-Brak, "The comorbidity of ADHD in children diagnosed with autism spectrum disorder," *Res. Autism Spectr. Disorders*, vol. 31, pp. 11–18, Nov. 2016.
[52] N. Rommelse, J. K. Buitelaar, and C. A. Hartman, "Structural brain imaging correlates of ASD and ADHD across the lifespan: A hypothesis-generating review on developmental ASD–ADHD subtypes," *J. Neural Transmiss.*, vol. 124, no. 2, pp. 259–271, Feb. 2017.

BYUNGGUN KIM received the B.E. and M.S. degrees in applied physics from Hanyang University, ERICA Campus, South Korea, in 2019 and 2021, respectively, where he is currently pursuing the Ph.D. degree in applied artificial intelligence. His current research interests include deep learning, rs-fMRI, and speech-emotion recognition.

JAESEON PARK received the B.E. degree in applied physics from Hanyang University, ERICA Campus, South Korea, in 2021, where he is currently pursuing the M.S. degree in applied artificial intelligence. His current research interests include deep learning, rs-fMRI, and speech-emotion recognition.

TAEHUN KIM received the B.E. degree in applied physics from Hanyang University (ERICA), Korea, in 2020 and M.S. degree in applied artificial intelligence from Hanyang University (ERICA), Korea, in 2022. He is currently with Konan Technology, South Korea. His current research interests include reinforcement learning and generative models.

YOUNGHUN KWON received the Ph.D. degree in theoretical physics from the University of Rochester, USA, in 1987. He is currently a Professor and the Head of the Department of Applied Physics, Hanyang University, South Korea. His current research interests include artificial intelligence for medical applications and speech emotion recognition, quantum machine learning, and quantum error correcting code for quantum computing.